

See discussions, stats, and author profiles for this publication at: <https://www.researchgate.net/publication/273443242>

# Protomers of Benzocaine: Solvent and Permittivity Dependence

ARTICLE in JOURNAL OF THE AMERICAN CHEMICAL SOCIETY · MARCH 2015

Impact Factor: 12.11 · DOI: 10.1021/jacs.5b01338

CITATIONS

8

READS

25

11 AUTHORS, INCLUDING:



Jasper Boschmans

Owlstone Nanotech Inc

3 PUBLICATIONS 14 CITATIONS

SEE PROFILE



W. Schöllkopf

Fritz Haber Institute of the Max Planck Society

46 PUBLICATIONS 1,122 CITATIONS

SEE PROFILE



Kevin Pagel

Freie Universität Berlin

30 PUBLICATIONS 564 CITATIONS

SEE PROFILE



Gert von Helden

Fritz Haber Institute of the Max Planck Society

190 PUBLICATIONS 8,252 CITATIONS

SEE PROFILE

# Protomers of Benzocaine: Solvent and Permittivity Dependence

Stephan Warnke,<sup>†</sup> Jongcheol Seo,<sup>†</sup> Jasper Boschmans,<sup>‡</sup> Frank Sobott,<sup>‡</sup> James H. Scrivens,<sup>§</sup> Christian Bleiholder,<sup>||</sup> Michael T. Bowers,<sup>||</sup> Sandy Gewinner,<sup>†</sup> Wieland Schöllkopf,<sup>†</sup> Kevin Pagel,<sup>\*,†</sup> and Gert von Helden<sup>\*,†</sup>

<sup>†</sup>Fritz-Haber-Institut der Max-Planck-Gesellschaft, Faradayweg 4-6, 14195 Berlin, Germany

<sup>‡</sup>Biomolecular and Analytical Mass Spectrometry Group, Department of Chemistry, University of Antwerp, Groenenborgerlaan 171, 2020 Antwerp, Belgium

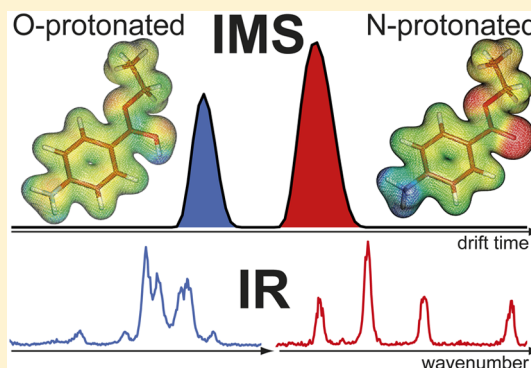
<sup>§</sup>School of Life Sciences, University of Warwick, Coventry CV47AL, United Kingdom

<sup>||</sup>Department of Chemistry and Biochemistry, University of California Santa Barbara, Santa Barbara, California 93106, United States

<sup>†</sup>Freie Universität Berlin, Institute of Chemistry and Biochemistry – Organic Chemistry, Takustrasse 3, 14195 Berlin, Germany

## Supporting Information

**ABSTRACT:** The immediate environment of a molecule can have a profound influence on its properties. Benzocaine, the ethyl ester of *para*-aminobenzoic acid that finds an application as a local anesthetic, is found to adopt in its protonated form at least two populations of distinct structures in the gas phase, and their relative intensities strongly depend on the properties of the solvent used in the electrospray ionization process. Here, we combine IR-vibrational spectroscopy with ion mobility–mass spectrometry to yield gas-phase IR spectra of simultaneously *m/z* and drift-time-resolved species of benzocaine. The results allow for an unambiguous identification of two protomeric species: the N- and O-protonated forms. Density functional theory calculations link these structures to the most stable solution and gas-phase structures, respectively, with the electric properties of the surrounding medium being the main determinant for the preferred protonation site. The fact that the N-protonated form of benzocaine can be found in the gas phase is owed to kinetic trapping of the solution-phase structure during transfer into the experimental setup. These observations confirm earlier studies on similar molecules where N- and O-protonation have been suggested.



## 1. INTRODUCTION

All atoms and molecules interact with their surroundings, which can be highly diverse ranging from a weakly interacting gas to a strongly interacting liquid or solid. The interactions of molecules with the environment will influence them by perturbing and shifting energy levels, thereby possibly altering their structures, reactivities, and other properties. Biological systems can offer a wide range of different environments. Those can be polar and protic in an aqueous medium or nonpolar and hydrophobic in a protein environment or inside a membrane. The corresponding relative permittivities  $\epsilon_r$  can range from  $\epsilon_r = 80$  for water to below  $\epsilon_r = 2$  in nonpolar surroundings. The different environments will have profound effects on the solubility, charge distribution, and the structures of molecules.

An interesting class of molecules, which are biologically active in (vastly) different dielectric environments, is comprised of the esters of *para*-aminobenzoic acid, some of which find a clinical application as local anesthetics (LAs).<sup>1,2</sup>

In contrast to aminobenzoic acid, which can act as both acid or base in aqueous solution, its esters are lacking an acidic group and can only act as a base, a common feature of all LAs.<sup>3</sup>

Their mode of action involves inhibition of signal conduction through the neuronal cell membrane by blocking the flux of  $\text{Na}^+$  ions through voltage-gated sodium channels.<sup>1,4–7</sup> In aqueous solutions at physiological conditions (pH 7.4, 150 mM NaCl), most LAs exist as both charged and neutral particles. However, the LA benzocaine (Figure 1), the ethyl ester of *para*-aminobenzoic acid, will not be protonated to an appreciable degree under these conditions because of its low  $\text{pK}_a$  value of 2.5. This property sets benzocaine apart from other LAs. In addition, the hydrophobic nature of benzocaine leads to a poor solubility in aqueous solutions at physiological conditions.<sup>8</sup> Despite these differences, benzocaine can still act as a sodium channel blocker, and the formation of a benzocaine– $\text{Na}^+$  complex inside the pore has been suggested to be the active form to solve this apparent paradox.<sup>9</sup>

For the analysis and identification of drugs and related compounds, mass spectrometry (MS)-based methods are indispensable today. To understand and quantify the results

Received: February 6, 2015

Published: March 11, 2015

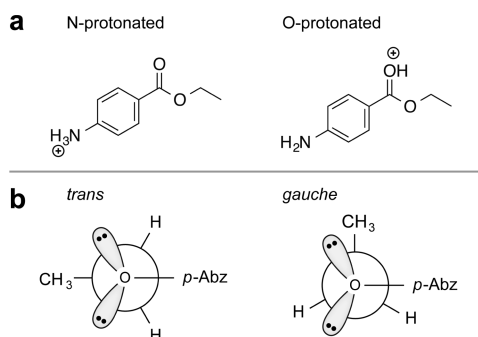


**Figure 1.** Potential sources of isomerism for protonated benzocaine. (a) Benzocaine can be protonated at the  $\text{NH}_2$  group (left) or the carbonyl oxygen (right). (b) In addition, trans/gauche isomers, in which the relative orientation of the ethyl group is altered, are conceivable. *p*-Abz denotes the position of the *p*-aminobenzoyl moiety.

obtained, it is important to find clear correlations between condensed-phase properties and those in the gas phase. Recent research is especially directed toward the implementation of ion mobility spectrometry (IMS), a method to separate different isobaric gas-phase structures, as a standard technique in conjunction with MS to aid compound analysis. In this context, it is essential to unambiguously link experimental and calculated results.

Here, we investigate the structure and protonation propensities of benzocaine when sprayed from solution into a solvent-free environment with relative permittivity,  $\epsilon_r$ , of 1. In terms of electric properties, such an environment resembles a hydrophobic membrane or the interior of a protein. We employ ion mobility–mass spectrometry (IM–MS) in conjunction with structure-sensitive spectroscopy in the mid-IR range using a free electron laser (FEL). With these methods, we probe the structure of benzocaine when electrosprayed from both protic and aprotic solvents with a goal of determining changes in the relative protomeric populations.

## 2. RESULTS AND DISCUSSION

**2.1. Ion Mobility–Mass Spectrometry of Singly Protonated Benzocaine.** IM–MS experiments were performed using an in-house-constructed drift-tube instrument (Figure 2) that has been described previously.<sup>10,11</sup> Ions are generated via nanoelectrospray ionization (nESI) and transferred into the low-pressure environment of the instrument. Here, ions are trapped, and short pulses are released into a nitrogen-filled drift region, which they traverse under the influence of a weak electric field at velocities that are related to

their corresponding size. Ions exiting the drift region are transferred into high vacuum where they are  $m/z$ -selected by a quadrupole mass filter and subsequently detected.

Figure 3a shows typical arrival time distributions (ATDs) of benzocaine electrosprayed from different solvents. Interestingly, two well-separated drift peaks can be observed, which change in relative intensity when the solvent composition is changed; a feature of high mobility with a drift time of 10.30 ms (**I**) is predominantly observed for an aqueous solution ( $\text{CH}_3\text{OH}/\text{H}_2\text{O}$ , lower panel) and a second, lower mobility feature at a drift time of 11.75 ms (**II**) is the strongest signal when the nonprotic solvent acetonitrile is used ( $\text{CH}_3\text{CN}$ , upper panel). Species **II** additionally exhibits a smaller unresolved component at a higher drift time (12.2 ms, **II'**).

The observation of two drift peaks that differ in drift time by approximately 14% is unusual for a molecule of this size and mass ( $m/z$  166) because it implies the coexistence of at least two isomers, vastly differing in size. The corresponding collision cross sections (CCSs) are determined to be 135 and 155 Å<sup>2</sup> for species **I** and **II**, respectively (Table 1 and Supporting Information). This difference in CCS must be a consequence of a difference in structure. From the chemical structure of benzocaine (Figure 1), very little structural diversity can be envisaged. The presence of trans and gauche isomers, which differ in the rotation angle of the ester group is conceivable (Figure 1b). However, such a rotation seems at the first glance rather unlikely to yield a drift-time difference of 14%. Another possibility is the formation of different protomers (Figure 1a), with the proton residing on either the amine nitrogen (N-protonated) or on the carbonyl oxygen (O-protonated). In aqueous solutions, the N-protonated species is certainly favored because of the basicity of the amino group, however, the situation can be very different in the absence of solvent molecules.<sup>12</sup> On the basis of results from studies where either (IM)–MS or spectroscopy have been employed independently, the existence of different gas-phase protomers has been suggested for smaller analogues of benzocaine, such as *para*-aminobenzoic acid<sup>13–15</sup> or *para*-hydroxybenzoic acid.<sup>16–18</sup> Also for these smaller systems with similar constituents and chemical structure, an influence of the solvent composition on the gas-phase ions has been reported, and evidence for both N- and O-protonated species was found.

**2.2. Drift-Time-Resolved IR Spectroscopy.** To gain further insight into the identity of the two species of benzocaine found in the IM–MS experiment, we recorded vibrational gas-phase spectra of the two isomers individually. Intramolecular vibrations strongly depend on the molecular structure, which makes vibrational spectroscopy, especially at frequencies in the

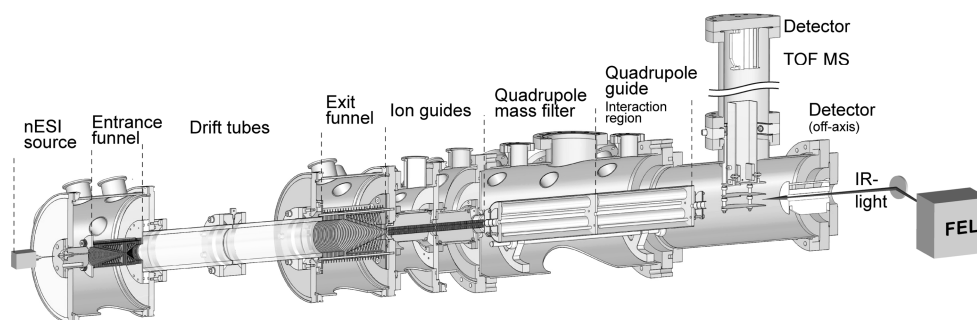


**Figure 2.** Schematic drawing of the drift-tube ion mobility–mass spectrometry experimental setup for mobility-selective gas-phase IR spectroscopy. Laser light coming from the free electron laser is coupled linearly into the setup using evacuated/nitrogen-flushed beamlines.

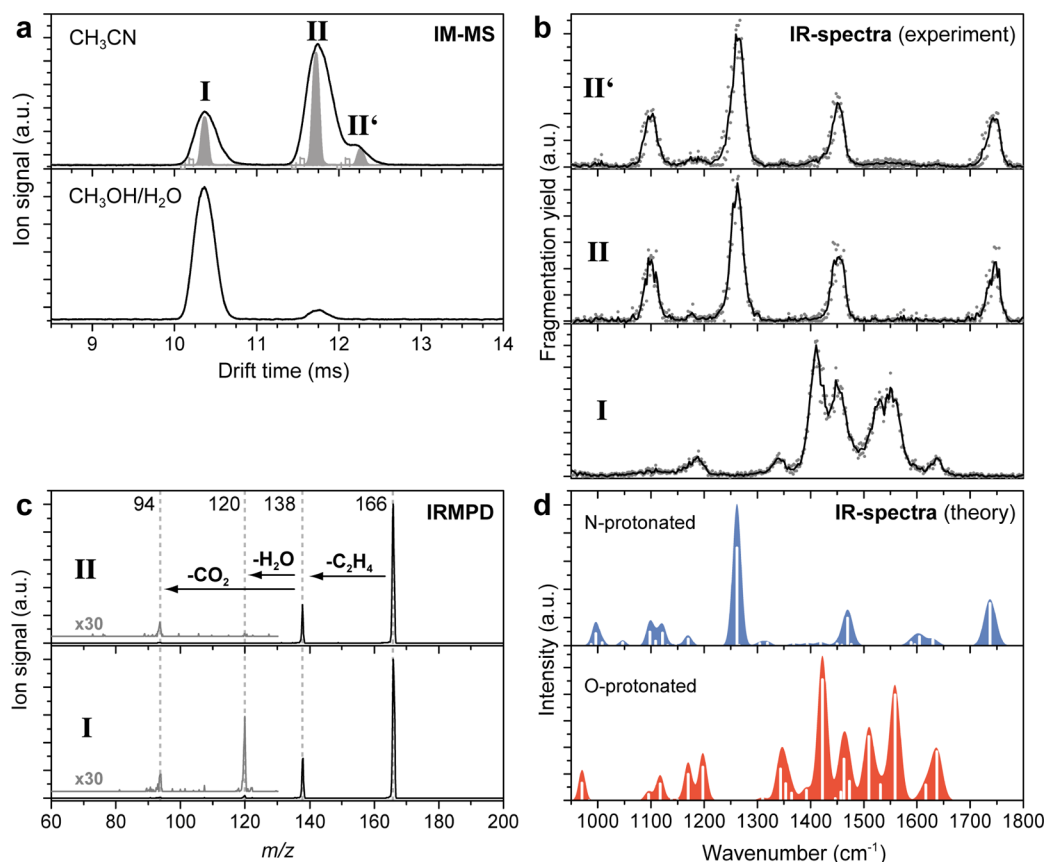


**Figure 3.** IR photofragmentation of drift-time-separated species of benzocaine ions. (a) Arrival time distributions (ATDs) of benzocaine, electrosprayed from acetonitrile (upper panel) and an aqueous solution (lower panel). The narrow 100  $\mu$ s signals (in gray) in the upper panel are the portions of the ATD transmitted for irradiation with IR photons. Each of these signals is preceded by a small rectangular signal, which stems from electrical noise. (b) Gas-phase IR spectra of the three species of benzocaine observed in the ATD. Data from two individual scans per species are depicted as gray dots. The solid lines represent an average of these two individual scans. (c) Photofragment spectra of species I and II. The identity of the fragments was confirmed by collision-induced dissociation experiments where identical fragmentation patterns were observed. (d) Computed vibrational spectra of the lowest-energy structures of N-protonated (upper panel) and O-protonated (lower panel) benzocaine ions. The theoretical spectra were scaled by a factor of 0.975 and convoluted with a Gaussian profile of 1.5% width to match the experiment.

**Table 1. Experimental and Theoretical CCSSs**

	CCS <sub>calc</sub> ( $\text{\AA}^2$ )		CCS <sub>exp</sub> ( $\text{\AA}^2$ )
	PSA <sup>a</sup>	TM <sup>b</sup>	
O-prot./trans	131.1	132.7	135
O-prot./gauche	131.6	132.5	
N-prot./trans	133.3	144.0	155
N-prot./gauche	129.5	144.0	

<sup>a</sup>Projection superposition approximation (PSA). <sup>b</sup>Trajectory method (TM).

mid-IR range, a valuable tool to deduce structural information. A common method to obtain IR spectra in the gas phase is to employ IR multiple photon dissociation (IRMPD) on  $m/z$ -selected ions.<sup>19</sup> Here, infrared lasers of high intensity are needed to allow for the absorption of multiple photons at IR-active sites, which results in increased internal energies and dissociation of covalent bonds. For these IRMPD experiments, the Fritz Haber Institute FEL is coupled to the IM-MS experimental setup, which enables spectroscopic investigation of drift-time separated species. Subsequent to drift-time and  $m/z$  separation, ions within a narrow drift-time window can be selected and irradiated by a pulse of intense IR light. Fragment analysis occurs by means of TOF MS. An action spectrum is recorded by monitoring the intensity of the precursor ion signal

and the corresponding fragment signals as a function of the laser wavelength.

The narrow (100  $\mu$ s) fractions of the ATD in the upper panel of Figure 3a are the fractions of species I, II, and II' that were isolated and transmitted for irradiation with IR photons following mass analysis. Typical IRMPD fragment spectra of species I and II at resonant wavelengths are depicted in Figure 3c. The most abundant fragment,  $m/z$  138 (loss of CO or C<sub>2</sub>H<sub>4</sub>), undergoes further fragmentation to yield substantially weaker fragment signals at  $m/z$  120 (loss of H<sub>2</sub>O) and  $m/z$  94 (loss of CO<sub>2</sub>). It is noteworthy that species II, which exhibits a lower dissociation yield than that of I, does not form the  $m/z$  120 fragment to a considerable extent. Similar fragmentation patterns are observed for II and II'. In addition, identical fragmentation behavior is observed when dissociation is induced via slow collisional heating. Fragment spectra obtained from collision-induced dissociation (CID) experiments resemble the IRMPD photofragment spectra in fragment types and relative abundances (Figure S1).

The resulting IR spectra in a wavenumber range of 950 to 1800  $\text{cm}^{-1}$  are presented in Figure 3b. The solid lines represent an average of two individual scans, which are depicted as gray dots. The spectra of I and II/II' are completely different. The latter set of spectra mainly consists of four strong bands at wavenumbers 1100, 1260, 1450, and 1745  $\text{cm}^{-1}$  with a width of



approximately  $25\text{ cm}^{-1}$  each, whereas the spectrum of **I** holds strong, partially resolved features between  $1375$  and  $1600\text{ cm}^{-1}$  and some weaker bands at  $1190$ ,  $1340$ , and  $1635\text{ cm}^{-1}$ .

To clarify the identities of species **I** and **II/II'**, it is crucial to assign the vibrational bands of the experimental spectra. We therefore computed model structures of benzocaine with N- and O-protonated sites as well as different orientations of the ethyl group (trans and gauche), which result from rotation of the ester bond (Figure 4). Theoretical spectra were calculated

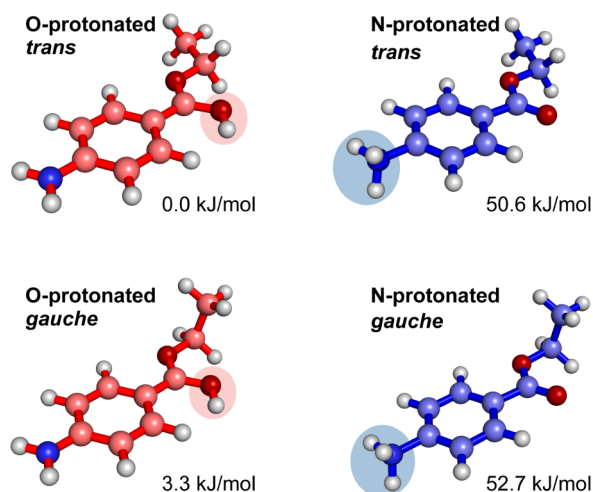


**Figure 4.** Calculated lowest-energy structures of O- and N-protonated benzocaine in trans and gauche conformation and corresponding relative energies. Structures were obtained using TURBOMOLE v6.6 at the B3LYP level of density functional theory with a def2-TZVP basis set.

using the B3LYP functional with the def2-TZVP basis set. For both protomers, the trans isomer is favored by  $2.1$ – $3.3\text{ kJ/mol}$  (Figure 4), and their most prominent vibrational bands are summarized in Tables S1 and S2. For comparison with experimental data, the calculated vibrational frequencies were scaled by a factor of  $0.975$  and convoluted with a Gaussian curve profile of  $1.5\%$  width. The resulting theoretical spectra are shown in Figure 3d in red for O-protonated (lower panel) and blue for N-protonated species (upper panel).

The theoretical spectrum of the N-protonated species is in excellent accord with the experimental spectra of **II** and **II'**, and all of the observed vibrations can be found in the predicted spectrum within the width of the experimental bands. Therefore, the observed bands at  $1745$  and  $1450\text{ cm}^{-1}$  can be assigned to  $\text{C}=\text{O}$  stretching and  $\text{NH}_3$  umbrella modes, respectively. More complex asymmetric and symmetric stretching vibrations of  $\text{C}-\text{C}$  and the ester-bonded ethyl group ( $\text{C}-\text{OEt}$ ) can be assigned to the observed bands at  $1260$  and  $1100\text{ cm}^{-1}$ , respectively. The nonlinear relation between laser power and band intensity in this multiple photon process is likely to be the reason for the absence of predicted lower-intensity vibrations in the experimental spectrum. The spectrum of species **I**, however, is in good agreement with the calculated spectrum of the O-protonated molecule. The individual vibrational modes, however, are mostly predicted to be not well-separated, which explains the more convoluted experimental spectrum. Nevertheless, a characteristic band in the spectrum of the O-protonated species, which arises from the stretching vibration of the protonated carbonyl ( $\text{C}=\text{OH}^+$ ) at  $1423\text{ cm}^{-1}$ , is particularly noteworthy because it can

exclusively be found in the experimental spectrum of **I**, whereas the band corresponding to the stretching vibration of the free carbonyl ( $\text{C}=\text{O}$ ) in an N-protonated molecule is absent. In summary, on the basis of the gas-phase IR spectra, the drift peaks **I** and **II/II'** in Figure 3a can unambiguously be assigned to O- and N-protonated species of benzocaine, respectively. Hypothetically, the molecule could also be protonated at the aromatic ring, as has been observed for protonated aniline.<sup>20</sup> For benzocaine, however, such structures are not energetically favorable nor do the experimental IR spectra show features characteristic for ring protonation, so they can therefore be excluded here (for details, see the Supporting Information).

The aforementioned differences in IRMPD- and CID-fragment spectra can now be explained on the basis of O- and N-protonated structures. The loss of water ( $m/z\ 120$ ), a feature observed in the fragment spectra of the O-protonated species **I**, is likely to be suppressed when the proton resides at the amide group and is therefore not observed in the fragment spectra of species **II/II'** (compare to Figure S2).

Identical fragmentation patterns and IR spectra are observed for species **II** and **II'**, which thus implies that both structures carry the charge at the amine nitrogen. Additionally, their difference in drift time implies a size difference of approximately  $4\%$ , which is unlikely to result from conformational changes considering the low flexibility of the molecule. ATDs from a commercial MS–IM–MS instrument do not exhibit this additional **II'** component (Figure S1). Unlike in this instrument, however, the here-utilized drift-tube instrument does not allow  $m/z$  selection prior to drift-time separation, and it is therefore possible that partially solvated N-protonated molecules traverse the drift tube and subsequently lose the weakly bound solvent molecules in the transfer region toward high vacuum before  $m/z$  selection occurs. These partially solvated benzocaine molecules will be larger than fully desolvated molecules and hence have slightly increased drift times, but they will be detected as fully desolvated molecules. This post-IM dissociation has been observed in earlier studies on drift-tube instruments and provides a reasonable explanation for the **II'** species.

**2.3. CCS Calculation.** After the unambiguous identification of the O- and N-protonated species of benzocaine, it remains to explain the baseline separation of these rather similar structures in the IM–MS experiment on the basis of the theoretical models. For this purpose, theoretical CCSs of the different protomers as well as their rotational trans and gauche isomers were calculated. Generally, several methods are available to achieve this, with the projection approximation (PA) method being the simplest.<sup>21,22</sup> In its standard form, a CCS is estimated by calculating the projected area (i.e., the shadow) of a molecule for many different orientations. A more refined version, the projection superposition approximation (PSA),<sup>23–26</sup> takes errors into account that arise from concave molecular structures and performs well for larger molecules. Effects that result from the charge distribution within the molecule, however, are ignored in these two methods. In the trajectory method (TM),<sup>27,28</sup> realistic ion–molecule interaction potentials, which can include charge-induced dipole interactions, are taken into account. This method is well-suited for smaller molecules such as benzocaine; however, it is of high computational cost for larger species.

Here, we calculated theoretical CCSs using the PSA and TM methods, which were both parametrized for nitrogen drift gas. Calculated CCSs of the trans and gauche conformers yield

virtually identical values, which is in stark contrast to the vastly differing experimental CCSs of 135 and 155 Å<sup>2</sup> for I and II, respectively (Table 1). Furthermore, the calculations suggest that the experimentally observed differences in drift time are likely a result of different electrostatic interactions with the nitrogen buffer gas molecules rather than distinct sizes of the structures. Although PSA calculations, which lack an explicit treatment of charge-induced interactions, yield essentially identical CCSs for all model structures, a difference in CCS of approximately 8% between the O- and N-protonated species is predicted by TM, which accounts for charge-induced dipole interactions. The theoretical CCS of the O-protonated model structure thus reproduces the experimental CCS of species I within the error of the method, whereas species II exhibits an experimental CCS that is still 6% higher than the calculated value of the N-protonated model structure. These results imply that the CCS calculation methods need to be further refined to account more thoroughly for charge effects in polarizable drift gases such as nitrogen. The underlying reason for a much longer drift time of the N-protonated species with respect to the O-protonated molecule is likely to be found in differences in the charge density distribution. A molecule with a more localized charge will experience a stronger interaction with the polarizable, neutral nitrogen molecules than a molecule with a delocalized charge, leading to longer drift times and higher CCSs in the IMS experiment. The former can be expected when the proton is located at the amide nitrogen, in contrast to an O-protonated benzocaine where the mesomeric effect leads to a more delocalized charge distribution.

**2.4. Influence of the Surrounding Medium.** The solvent composition has been observed to have a great influence on relative abundances of the electrosprayed O- and N-protonated species of benzocaine in the gas phase. A methanol/water solution facilitates protonation at the carbonyl oxygen, whereas species with a protonated amine are predominantly observed when acetonitrile is used as a solvent. These observations are in line with previous findings on the influence of the solvent on the gas-phase structures of positively and negatively charged smaller analogs of benzocaine.<sup>13,14,17,18</sup>

To shed more light on the influence of the surrounding media on the molecular structure, we calculated proton affinities,  $E_{\text{pa}}$ , of O- and N-protonated species of benzocaine as a function of the medium's relative permittivity  $\epsilon_r$  (Figure 5). These calculations suggest that in a polar solution protonation

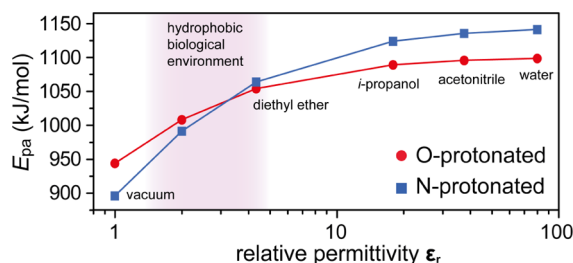


**Figure 5.** Proton affinity of N- and O-protonated species. Single-point energies of the lowest-energy structures of N- and O-protonated benzocaine were calculated for different relative permittivities  $\epsilon_r$  of the surrounding media and subtracted from the energy of the neutral molecule to yield the negative of the proton affinity,  $-E_{\text{pa}}$ . Solvated in water, the proton will be attached to the amide nitrogen, whereas carbonyl-oxygen protonation is favored in environments of lower relative permittivity.

will most likely occur at the amine rather than the ester group (up to 50 kJ/mol more stable). Considering the  $\text{pK}_a$  value of the amino group, this is the expected behavior for the molecule in an aqueous solution. When the relative permittivity of the surrounding medium decreases, however, the carbonyl oxygen becomes the preferred protonation site. This can be attributed to a conjugation between the amine and the charged carbonyl group in the absence of solvent molecules.<sup>29,30</sup> The electron-density-donating neutral amine and the density-withdrawing positively charged ester group both work in favor of the conjugated  $\pi$  system, thus stabilizing protonation at the carbonyl oxygen.

If protonation at the oxygen is favored under vacuum conditions, then why are both protomers observed in the gas phase and why does their relative abundance depend on the solvent medium? The observation of energetically unfavored N-protonated species in the gas phase (by 50 kJ/mol) must be a consequence of the electrospray process. In the electrospray process, the molecule undergoes a transition from a solvated to a desolvated state. When a protic solvent as methanol/water is used, the presence of many protic solvent molecules facilitate relocation of the charge to the preferred site within the last solvation shell; hence, the O-protonated species can be observed. However, an aprotic solvent like acetonitrile does not allow this structural reorganization in the last steps of the transition from solution to the gas phase, and the solution structure is therefore kinetically trapped,<sup>13,14,30</sup> leading to the formation of N-protonated benzocaine. Nonetheless, O-protonation can be facilitated by residual water inside the aprotic solvent.

These results can also be interpreted from a physiological point of view. Benzocaine is known to act as a local anesthetic by blocking sodium channels.<sup>1,4,6,7</sup> The majority of sodium channel blockers act as charged molecules, blocking the transit of  $\text{Na}^+$  ions inside the pore, whereas benzocaine is commonly assumed to act as a neutral.<sup>1,4,6,7</sup> However, the proton affinity of benzocaine is dependent on the permittivity of the surrounding medium. The estimated relative permittivity of a lipid bilayer or a transmembrane protein is estimated to be  $\epsilon_r \approx 2-6$ , which is much smaller than typical for in vitro conditions (Figure 5). Whether benzocaine acts on the sodium channel as a charged or neutral molecule cannot be deduced from the experiments presented here. However, if protonation plays a role in the underlying mechanism, then the proton will most likely be located at the carbonyl oxygen because of the hydrophobicity of the ion channel.

### 3. CONCLUSIONS

Ion-mobility-resolved IR spectroscopy provides the first direct evidence for different protomeric populations of the local anesthetic benzocaine, the ethyl ester of *para*-aminobenzoic acid. At least two well-separable gas-phase species can be found in IM-MS experiments. Vibrational spectra of these both  $m/z$ -as well as ion-mobility-selected species were recorded in the mid-IR range using a free electron laser, and two different protomers, O- and N-protonated benzocaine, were unambiguously identified by comparison with calculated spectra from density functional theory calculations. Distinct photofragmentation and collision-induced dissociation fragment patterns as well as calculated collision cross sections of model structures further support the structural assignment. For the latter the incorporation of charge-induced dipole terms is crucial because the differences in drift time of the two species do not arise from

their conformational diversity but rather from different charge distribution within the molecules. Our results confirm earlier studies on structurally similar molecules where the existence of different gas-phase protomers was suggested.<sup>13,14,17,18,31</sup>

Calculated proton affinities further suggest that the preferred protonation site may vary significantly with the electric properties of the surrounding medium. Although the amide nitrogen is the most basic site in aqueous environments, the carbonyl oxygen becomes energetically favorable for protonation when the relative permittivity decreases. Consequently, a protic solvent, such as water/methanol, facilitates rearrangement of the proton to the preferred site on the way from the ion source into the gas-phase, whereas an aprotic solvent leads to kinetic trapping of the most stable solution structure.<sup>13,14,30</sup> These results may have an impact on studies of molecules as benzocaine in hydrophobic environments, such as a membranes or ion channels, which in terms of relative permittivity,  $\epsilon_r$ , resemble the gas phase more than an aqueous solution.

## 4. MATERIALS AND METHODS

**4.1. Samples.** Benzocaine and all solvents were purchased from Sigma-Aldrich (Taufkirchen, Germany) and used without further purification. Solutions of 100  $\mu\text{M}$  benzocaine were prepared with water/methanol (v/v, 50:50) and pure acetonitrile as solvents, respectively. For (nano)electrospray ionization,  $\sim 5\ \mu\text{L}$  of sample were loaded into in-house-prepared Pd–Pt-coated borosilicate capillaries, and voltages of 0.8–1.0 kV were applied.

**4.2. Isomer-Selective IR Spectroscopy.** The ion mobility method for drift-time-based selection is well established.<sup>32</sup> To preselect gas-phase isomers prior to irradiation with intense IR light, an in-house-constructed drift-tube ion mobility–mass spectrometer similar to one described previously was used.<sup>10,11</sup> Figure 2 depicts a schematic drawing of the experimental setup. Ions are generated in a (nano)electrospray ionization source and transferred into the vacuum environment of the experimental apparatus. An electrodynamic ion funnel (entrance funnel) collects ions and releases 150  $\mu\text{s}$  pulses into the nitrogen-filled drift tube (5 mbar), which they traverse under the influence of a weak electric field ( $\sim 10\ \text{V/cm}$ ). A second electrodynamic funnel (exit funnel) collects the ion clouds and guides them through a 0.5 mm orifice into a differentially pumped region, where ion guides transport them into a high vacuum region. Here,  $m/z$  selection occurs in a quadrupole mass filter and arrival time distributions (ATDs) can be recorded by measuring the time dependent ion current of the  $m/z$  selected species after release of the ion trap.

For isomer-selective irradiation with IR light, a narrow drift-time window of 100  $\mu\text{s}$  width can be selected by electrostatic deflection prior mass selection. These  $m/z$  and drift-time/ionomer selected ions then traverse a quadrupole guide and are irradiated by a 10  $\mu\text{s}$  pulse of IR photons with typical pulse energies between 10 and 40 mJ. The wavelength-dependent photofragmentation is monitored by means of TOF MS, and IR spectra are composed by computing the fragmentation yield for each wavelength step.

IR light is generated by a free electron laser<sup>33</sup> housed in the Fritz Haber Institute and transported through an evacuated beamline until it reaches the experimental setup. For practical reasons, the last two meters of the beamline, which is directly connected to the instrument, is flushed with dry nitrogen to avoid water absorption.

**4.3. Computational Methods.** Optimized geometries, relative energies, and harmonic vibrational frequencies of O- and N-protonated benzocaine were calculated at the B3LYP level of density functional theory with a def2-TZVP basis set using TURBOMOLE v6.6.<sup>34</sup> Vibrational frequencies are scaled by a factor of 0.975 and convoluted with a Gaussian profile of 1.5% width to fit the experimental spectra. Proton affinities  $E_{\text{pa}}$  were calculated by determining single-point energies of the lowest-energy structures of the O- and N-protonated species, using the COSMO solvation model<sup>35</sup> for different relative permittivities,  $\epsilon_r$ , of the surrounding media and subsequent subtraction from the energy of the neutral.

## ■ ASSOCIATED CONTENT

### Supporting Information

Experimental procedures, data from drift-time selective collision induced dissociation experiments, fragmentation pathways, most intense calculated vibrational frequencies, and theoretical spectra of ring-protonated benzocaine. This material is available free of charge via the Internet at <http://pubs.acs.org>.

## ■ AUTHOR INFORMATION

### Corresponding Authors

\*helden@fhi-berlin.mpg.de

\*kevin.pagel@fu-berlin.de

### Present Address

C.B.: Department of Chemistry, Florida State University, Tallahassee, Florida 32306–4390.

### Notes

The authors declare no competing financial interest.

## ■ ACKNOWLEDGMENTS

M.T.B. gratefully acknowledges support from the US National Science Foundation under grant no. CHE-1301032 and the Alexander von Humboldt foundation.

## ■ REFERENCES

- (1) Hille, B. *J. Gen. Physiol.* **1977**, *69*, 497.
- (2) Schwarz, H.; Palade, P.; Hille, B. *Biophys. J.* **1977**, *20*, 343.
- (3) Nardi, A.; Damann, N.; Hertrampf, T.; Kless, A. *ChemMedChem* **2012**, *7*, 1712.
- (4) Schwarz, W.; Palade, P. T.; Hille, B. *Biophys. J.* **1977**, *20*, 343.
- (5) Hille, B. *Ion Channels of Excitable Membranes*; 3rd ed.; Sinauer Associates: Sunderland, MA, 2001.
- (6) Lipkind, G. M.; Fozzard, H. A. *Mol. Pharmacol.* **2005**, *68*, 1611.
- (7) Boiteux, C.; Vorobyov, I.; French, R. J.; French, C.; Yarov-Yarovoy, V.; Allen, T. W. *Proc. Natl. Acad. Sci. U.S.A.* **2014**, *111*, 13057.
- (8) Ávila, C. M.; Martínez, F. *J. Solution Chem.* **2002**, *31*, 975.
- (9) Tikhonov, D. B.; Bruhova, I.; Zhorov, B. S. *FEBS Lett.* **2006**, *580*, 6027.
- (10) Kemper, P. R.; Dupuis, N. F.; Bowers, M. T. *Int. J. Mass Spectrom.* **2009**, *287*, 46.
- (11) Warnke, S.; Baldauf, C.; Bowers, M. T.; Pagel, K.; von Helden, G. *J. Am. Chem. Soc.* **2014**, *136*, 10308.
- (12) Kebarle, P.; Peschke, M. *Anal. Chim. Acta* **2000**, *406*, 11.
- (13) Tian, Z.; Kass, S. R. *Angew. Chem.* **2009**, *121*, 1347.
- (14) Schmidt, J.; Meyer, M. M.; Spector, I.; Kass, S. R. *J. Phys. Chem. A* **2011**, *115*, 7625.
- (15) Campbell, J. L.; Le Blanc, J. C.; Schneider, B. B. *Anal. Chem.* **2012**, *84*, 7857.
- (16) Tian, Z.; Wang, X. B.; Wang, L. S.; Kass, S. R. *J. Am. Chem. Soc.* **2009**, *131*, 1174.
- (17) Steill, J. D.; Oomens, J. *J. Am. Chem. Soc.* **2009**, *131*, 13570.
- (18) Schröder, D.; Budesinsky, M.; Roithova, J. *J. Am. Chem. Soc.* **2012**, *134*, 15897.



- (19) Oomens, J.; Sartakov, B. G.; Meijer, G.; von Helden, G. *Int. J. Mass Spectrom.* **2006**, *254*, 1.
- (20) Lalli, P. M.; Iglesias, B. A.; Toma, H. E.; de Sa, G. F.; Daroda, R. J.; Silva Filho, J. C.; Szulejko, J. E.; Araki, K.; Eberlin, M. N. *J. Mass Spectrom.* **2012**, *47*, 712.
- (21) von Helden, G.; Hsu, M. T.; Gotts, N.; Bowers, M. T. *J. Phys. Chem.* **1993**, *97*, 8182.
- (22) Wyttenbach, T.; Helden, G.; Batka, J. J.; Carlat, D.; Bowers, M. T. *J. Am. Soc. Mass Spectrom.* **1997**, *8*, 275.
- (23) Bleiholder, C.; Wyttenbach, T.; Bowers, M. T. *Int. J. Mass Spectrom.* **2011**, *308*, 1.
- (24) Anderson, S. E.; Bleiholder, C.; Brocker, E. R.; Stang, P. J.; Bowers, M. T. *Int. J. Mass Spectrom.* **2012**, *330–332*, 78.
- (25) Bleiholder, C.; Contreras, S.; Do, T. D.; Bowers, M. T. *Int. J. Mass Spectrom.* **2013**, *345–347*, 89.
- (26) Bleiholder, C.; Contreras, S.; Bowers, M. T. *Int. J. Mass Spectrom.* **2013**, *354–355*, 275.
- (27) Mesleh, M. F.; Hunter, J. M.; Shvartsburg, A. A.; Schatz, G. C.; Jarrold, M. F. *J. Phys. Chem.* **1996**, *100*, 16082.
- (28) Campuzano, I.; Bush, M. F.; Robinson, C. V.; Beaumont, C.; Richardson, K.; Kim, H.; Kim, H. I. *Anal. Chem.* **2012**, *84*, 1026.
- (29) Tang, M.; Isbell, J.; Hodges, B.; Brodbelt, J. *J. Mass Spectrom.* **1995**, *30*, 977.
- (30) Chang, T. M.; Prell, J. S.; Warrick, E. R.; Williams, E. R. *J. Am. Chem. Soc.* **2012**, *134*, 15805.
- (31) Laphorn, C.; Dines, T. J.; Chowdhry, B. Z.; Perkins, G. L.; Pullen, F. S. *Rapid Commun. Mass Spectrom.* **2013**, *27*, 2399.
- (32) Bowers, M. T. *Int. J. Mass Spectrom.* **2014**, *370*, 75.
- (33) Schöllkopf, W.; Erlebach, W.; Gewinner, S.; Heyne, G.; Junkes, H.; Liedke, A.; Meijer, G.; Platschkowski, V.; von Helden, G.; Bluem, H.; Dowell, D.; Lange, R.; Rathke, J.; Todd, A. M. M.; Young, L. M.; Lehnert, U.; Michel, P.; Seidel, W.; Wunsch, R.; Gottschalk, S. C. The New IR FEL Facility at the Fritz-Haber-Institut in Berlin. *Proceedings of FEL 2014*, Basel, Switzerland, August 25–29, 2014; WEB04.
- (34) University of Karlsruhe and Forschungszentrum Karlsruhe GmbH *TURBOMOLE*, v6.6 2014; *TURBOMOLE GmbH*: Karlsruhe, Germany, 2014; available from <http://www.turbomole.com>.
- (35) Klamt, A.; Schüürmann, G. *J. Chem. Soc., Perkin Trans. 2* **1993**, 799.